Cell

A Nuclear Pyruvate Dehydrogenase Complex Is Important for the Generation of Acetyl-CoA and Histone Acetylation

Gopinath Sutendra,[1,3,*] Adam Kinnaird,[1] Peter Dromparis,[1] Roxane Paulin,[1] Trevor H. Stenson,[1] Alois Haromy,[1] Kyoko Hashimoto,[1] Nancy Zhang,[2] Eric Flaim,[2] and Evangelos D. Michelakis[1,*]
[1]Department of Medicine
[2]nanoFAB Fabrication and Characterization Facility
University of Alberta, Edmonton, AB T6G 2B7, Canada
[3]Present address: Ludwig Institute for Cancer Research, Nuffield Department of Clinical Medicine, University of Oxford, Oxford OX3 7DQ, UK
*Correspondence: gopinath.sutendra@ludwig.ox.ac.uk (G.S.), em2@ualberta.ca (E.D.M.)
http://dx.doi.org/10.1016/j.cell.2014.04.046

SUMMARY

DNA transcription, replication, and repair are regulated by histone acetylation, a process that requires the generation of acetyl-coenzyme A (CoA). Here, we show that all the subunits of the mitochondrial pyruvate dehydrogenase complex (PDC) are also present and functional in the nucleus of mammalian cells. We found that knockdown of nuclear PDC in isolated functional nuclei decreased the de novo synthesis of acetyl-CoA and acetylation of core histones. Nuclear PDC levels increased in a cell-cycle-dependent manner and in response to serum, epidermal growth factor, or mitochondrial stress; this was accompanied by a corresponding decrease in mitochondrial PDC levels, suggesting a translocation from the mitochondria to the nucleus. Inhibition of nuclear PDC decreased acetylation of specific lysine residues on histones important for G1-S phase progression and expression of S phase markers. Dynamic translocation of mitochondrial PDC to the nucleus provides a pathway for nuclear acetyl-CoA synthesis required for histone acetylation and epigenetic regulation.

INTRODUCTION

Epigenetic regulation of gene expression is essential for embryonic development and differentiation, protection against viruses, and progression of cancer (Jaenisch and Bird, 2003). It includes modifications of core histones by either methylation or acetylation. By neutralizing the positive charges of lysine residues in histones, acetylation promotes the relaxation of DNA, necessary for replication and transcription (Vogelauer et al., 2002). A recent high-resolution mass spectrometry analysis identified a large number of nuclear proteins with multiple acetylation sites, suggesting that the role of acetylation extends beyond histones (Choudhary et al., 2009). In eukaryotes, the biosynthesis of acetyl-coenzyme A (CoA) is thought to occur in the subcellular compartment where it is required, because it is membrane impermeable and very unstable, due to the high-energy thioester bond that joins the acetyl and CoA groups. Our understanding of how the nucleus generates acetyl-CoA in metazoan cells is incomplete. Acetyl-CoA synthetase (AceCS1) and ATP-citrate lyase (ACL) are both present in the nucleus (Wellen et al., 2009). ACL is the predominant pathway for nuclear acetyl-CoA generation in mammalian cells because it utilizes glucose-oxidation-derived mitochondrial citrate as its substrate, as opposed to AceCS1, which uses acetate, a fuel that is not an important energy source for mammalian cells (Wellen et al., 2009). However, in cells with decreased citrate levels due to mitochondrial suppression by Bcl-xL overexpression, levels of acetyl-CoA and N-α-acetylated proteins decreased in the cytoplasm with no apparent decrease in histone acetylation (Yi et al., 2011). This suggested the presence of a yet unidentified mitochondria-independent mechanism for histone acetylation in the nucleus.

Primitive protozoan cells that lack mitochondria, like *Entamoeba histolytica*, utilize pyruvate:ferrodoxin oxidoreductase (PFO) to generate acetyl-CoA (Rodríguez et al., 1998). Mammalian cells do not express PFO but generate acetyl-CoA in mitochondria with a similar complex of nucleus-encoded proteins known as pyruvate dehydrogenase complex (PDC) (Horner et al., 1999). The generation of acetyl-CoA from both PFO and PDC is dependent on the glycolysis-derived product pyruvate. The nuclear presence of several metabolic enzymes has been observed as early as the 1960s, with many shown to interact with nuclear proteins and DNA and "moonlight" to the nucleus in conditions of cellular stress (Kim and Dang, 2005; Siebert and Humphrey, 1965; Yang et al., 2012; Yogev et al., 2010). For example, the M2 isoform of the glycolytic enzyme pyruvate kinase (PKM2) translocates to the nucleus and functions as a protein kinase, phosphorylating nuclear proteins, like threonine-11 of histone 3 (H3), and enhancing the acetylation of lysine 9 on H3 (H3K9) (Yang et al., 2012). The protein kinase function of PKM2 utilizes the glycolytic intermediate phosphoenolpyruvate (PEP) and not ATP as its phosphate donor (Vander Heiden et al., 2010), resulting in the subsequent generation of pyruvate

(Gao et al., 2012; Yang et al., 2012). However, the fate of pyruvate in the nucleus and whether this is related to the acetyl-CoA used in the H3K9 acetylation remain unknown.

Intact and functional PDC can translocate across mitochondrial membranes from the matrix to the outer mitochondrial membrane (Hitosugi et al., 2011). Thus, it would be possible for a chaperone protein to bind PDC from the outer mitochondrial membrane and bring it to the nucleus under conditions that stimulate S phase entry and cell-cycle progression, where histone acetylation is critical.

We provide evidence that supports the hypothesis that functional PDC can translocate from the mitochondria to the nucleus during cell-cycle progression, generating a nuclear pool of acetyl-CoA from pyruvate and increasing the acetylation of core histones important for S phase entry. The mitochondrial pyruvate dehydrogenase kinase (PDK), which phosphorylates and inhibits mitochondrial PDC, was not detectable in the nucleus, suggesting that nuclear PDC may be constitutively active and regulated differently than mitochondrial PDC. The nuclear translocation of PDC was triggered by growth signals, like serum and epidermal growth factor, or mitochondrial inhibitors, like rotenone. Nuclear PDC provides a means for the nucleus to generate acetyl-CoA in an autonomous fashion. The implications of this work extend to many conditions where nuclear acetylation is altered, like development, cancer, neurodegeneration, or cardiovascular disease.

RESULTS

All Components of PDC Are Present in the Nucleus

PDC is comprised of subunits from three catalytic enzymes: pyruvate dehydrogenase (E1), dihydrolipoamide transacetylase (E2), and dihydrolipoamide dehydrogenase (E3), as well as the tethering protein, E3-binding protein (E3BP) (Behal et al., 1993). We first identified the nuclear presence of PDC-E1 (α subunit) in human spermatozoa, which compartmentalize the nucleus (in the head) away from mitochondria (in the midsection), allowing for more clear visualization of nuclear versus mitochondrial PDC (Figure S1A available online). To confirm the nuclear presence of PDC-E1 in a terminally differentiated primary cell line, we isolated primary fibroblasts from human lungs and detected its nuclear presence (Figure 1A). We then performed a more-detailed assessment for the presence of nuclear PDC using microscopy in two commercially available cell lines, normal small airway epithelial cells (SAEC) and A549 cells (non-small-cell lung cancer cells). In intact SAEC and A549 cells costained with an antibody against PDC-E1 and the mitochondrial marker MitoTracker Red, colocalization of the two signals was evident in the cytoplasm as expected, but PDC-E1 was also evident within the nucleus (marked by DAPI) without any mitochondrial signal (Figures 1B and 1C). For our imaging, we generated 25 separate images in each intact cell, systematically scanning in the z axis at 0.2 μm in depth for each image. We used these stacked images to generate 3D videos that show the presence of PDC-E1 throughout the nucleus (Movies S1 and S2). We selected specific planes that ''cut through the nucleus'' from the z stacked images, as shown in the top image of Figure 1D. Then, in the XY axis, we quantified the nuclear PDC-E1 and MitoTracker Red signals by measuring the fluorescence intensity. As we move from left to right in the image plane, an area of mitochondria is followed by an area where only the nucleus is present. PDC-E1 is highly detected in the mitochondria and colocalizes with the MitoTracker Red signal. However, whereas the MitoTracker Red signal intensity is absent in the nucleus, the PDC-E1 signal is present, though with lesser intensity than the mitochondrial PDC-E1 signal (Figure 1D). Furthermore, nuclear PDC-E1 followed a similar signal pattern to the nuclear protein histone 3, confirming the specificity of the nuclear PDC-E1 signal (Figure S1B). In addition, a clear nuclear signal of PDC-E1 was also detected in the nucleus using electron microscopy (Figure S1C). These data show that the nuclear PDC-E1 signal is not a ''contamination'' from overlapping mitochondria.

To address the possibility that our PDC-E1 antibody nonspecifically binds to other nuclear proteins, we transfected A549 and SAEC with a plasmid encoding for cloned human E1α subunit of PDC in frame with enhanced GFP (EGFP). Based on EGFP fluorescence, we detected the presence of the fused EGFP-E1 protein in mitochondria as well as the nucleus of both cell types (Figures 1E and S1D). We then identified the nuclear presence for other subunits of the PDC complex, including PDC-E2, PDC-E3, and the ancillary subunit PDC-E3BP in intact cells using immunofluorescence (Figures 1F–1H). For all confocal and electron microscopy experiments, a ''secondary antibody-only'' control staining was performed, which in all experiments showed no signal (Figure S1E).

Nuclear PDC Is Functional and Can Generate Acetyl-CoA from Pyruvate

To assess if nuclear PDC is functional, we isolated nuclei using a nuclei-specific, high-sucrose gradient centrifugation protocol. As even a small amount of mitochondrial membranes could be a confounding factor, we took several steps to ensure that our nuclei were not contaminated with any mitochondria. We showed that nuclear membranes were intact by the lamin-staining pattern and that our nuclear preparations were free of mitochondrial membranes, as assessed by nonyl-acridine orange (NAO) and MitoTracker Red imaging (Figures 2A and 2B), as well as free of cytoplasmic, mitochondrial matrix, and membrane proteins, as assessed by immunoblots with antibodies against α-tubulin, citrate synthase (CS), isocitrate dehydrogenase 2 (IDH2), succinyl-CoA synthetase (SCS), and succinate dehydrogenase (SDH) (Figure 2C). These vigorous purity indices were used in all of our experiments with isolated nuclear preparations throughout this work. In these pure nuclei preparations, we confirmed the presence of PDC-E1 in nuclei from the EGFP-transfected cells, as well as from intact nuclei from A549 and SAEC cells, using immunofluorescence, with absence of any detectable signal in secondary-only antibody straining (Figure S2A, upper panels). In addition to the α subunit of the PDC-E1, all the subunits of the PDC complex were present in isolated nuclei (Figure S2A, bottom panels). We then used immunoblots and showed the nuclear presence of all PDC subunits in isolated nuclei from A549 cells (Figure 2D) as well as a separate cancer cell line, 786-O renal cell

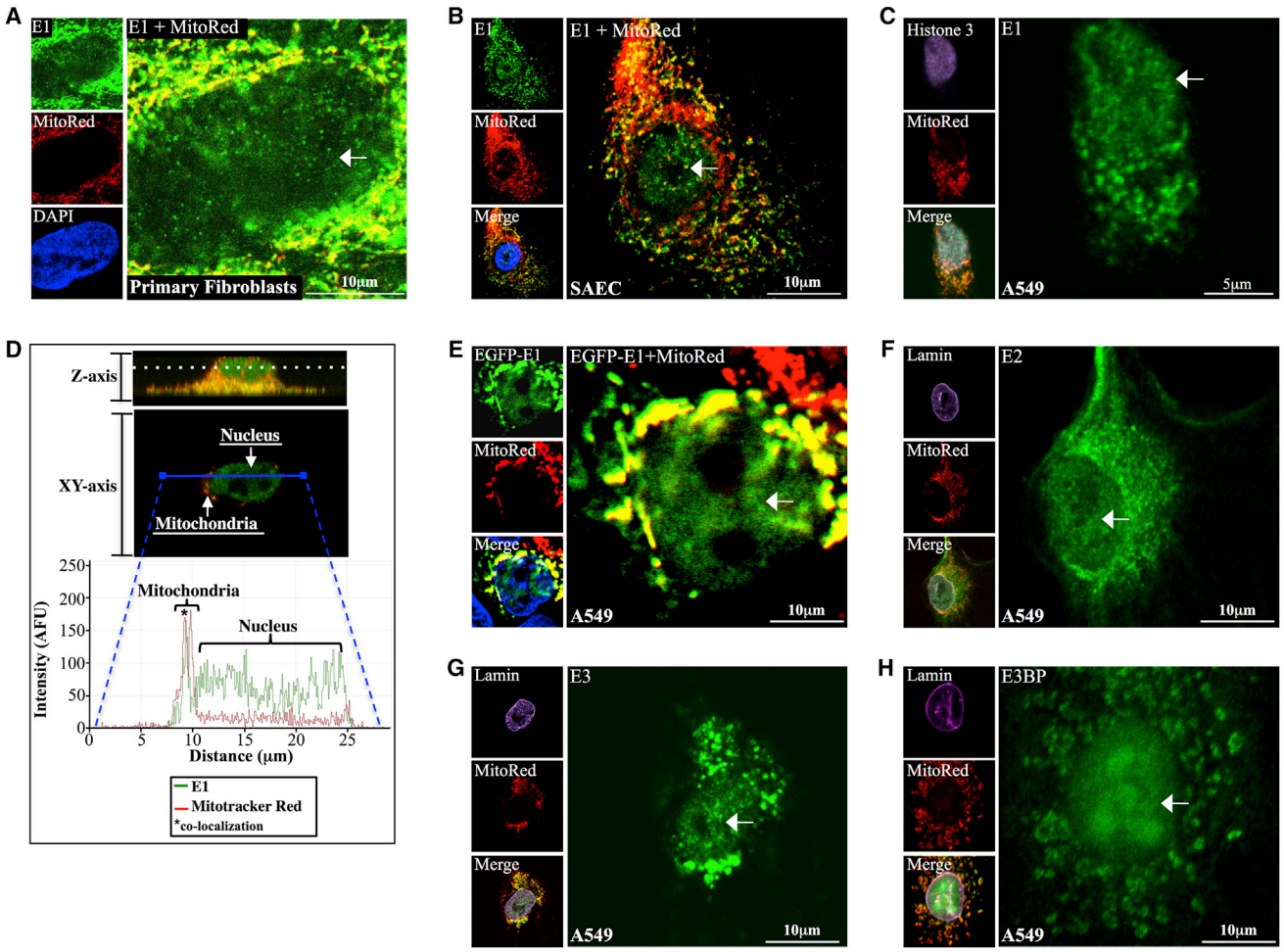

Figure 1. PDC Is Present in the Nucleus of Human Cells

(A–C) Primary fibroblasts (A), small airway epithelial cells (SAECs) (B), and A549 cells (C) were costained with an antibody to the α subunit of PDC-E1 (green), the mitochondrial marker MitoTracker Red (red), and either the nuclear marker DAPI (blue for A and B) or histone 3 (purple for C). The arrow shows PDC-E1 localized in the nucleus in the absence of a mitochondrial signal.

(D) An A549 cell was costained with PDC-E1 (green) and MitoTracker Red (red) and scanned at 0.2 μm increments along the z axis using confocal microscopy (top image). The fluorescence intensities midlane in the cell in the XY axis are shown (top and middle images).

(E) A549 cells were transfected with a plasmid encoding for EGFP-PDC-E1 and costained with MitoTracker Red and DAPI. EGFP-PDC-E1 is clearly seen in the nucleus (white arrow).

(F–H) A549 cells were costained with PDC-E2 (F), PDC-E3 (G), and PDC-E3BP (H) (all in green); MitoTracker Red; and lamin (purple). The images were taken at the midplane of the cell and clearly show the nuclear presence of PDC (white arrow).

See also Figure S1.

carcinoma cells, in the absence of cytoplasmic or mitochondrial contamination (Figure 2E). As NAD(H) is abundant in the nucleus, our finding that PDC-E2 appears to be lipoylated (implying the nuclear presence of lipoic acid; not present in our media), suggests that nuclear PDC has all the necessary cofactors to be functional (Figure S2B).

To study the function of nuclear PDC without interference from mitochondrial PDC, we performed our initial experiments on isolated nuclei. We detected many glycolytic intermediates, including PEP, pyruvate, and acetyl-CoA, using collision-induced dissociation mass spectrometry (Figure 2F). We then designed an experiment to study whether nuclear PDC is functional in terms of the de novo biosynthesis of acetyl-CoA.

We first isolated intact and pure nuclei from either A549 or 786-O cells previously treated with scrambled versus PDC-E1 small interfering RNA (siRNA). We obtained an efficient knockdown of PDC-E1, resulting in no detectable immunoblot signal (Figure 2G, top). This was in keeping with the absence of any PDC activity in nuclei lacking PDC, measured by a standard dipstick assay that measures the NADH produced by the immunocaptured enzyme (Figure 2G, bottom).

We then treated these nuclei with an isotope-labeled form of pyruvate ($^{13}C_2$-pyruvate) for 8 hr and measured the production of labeled acetyl-CoA ($^{13}C_1$-acetyl-CoA; Figure 2H). Because the only way to synthesize acetyl-CoA from pyruvate is by PDC, the detection of labeled acetyl-CoA in our nuclear

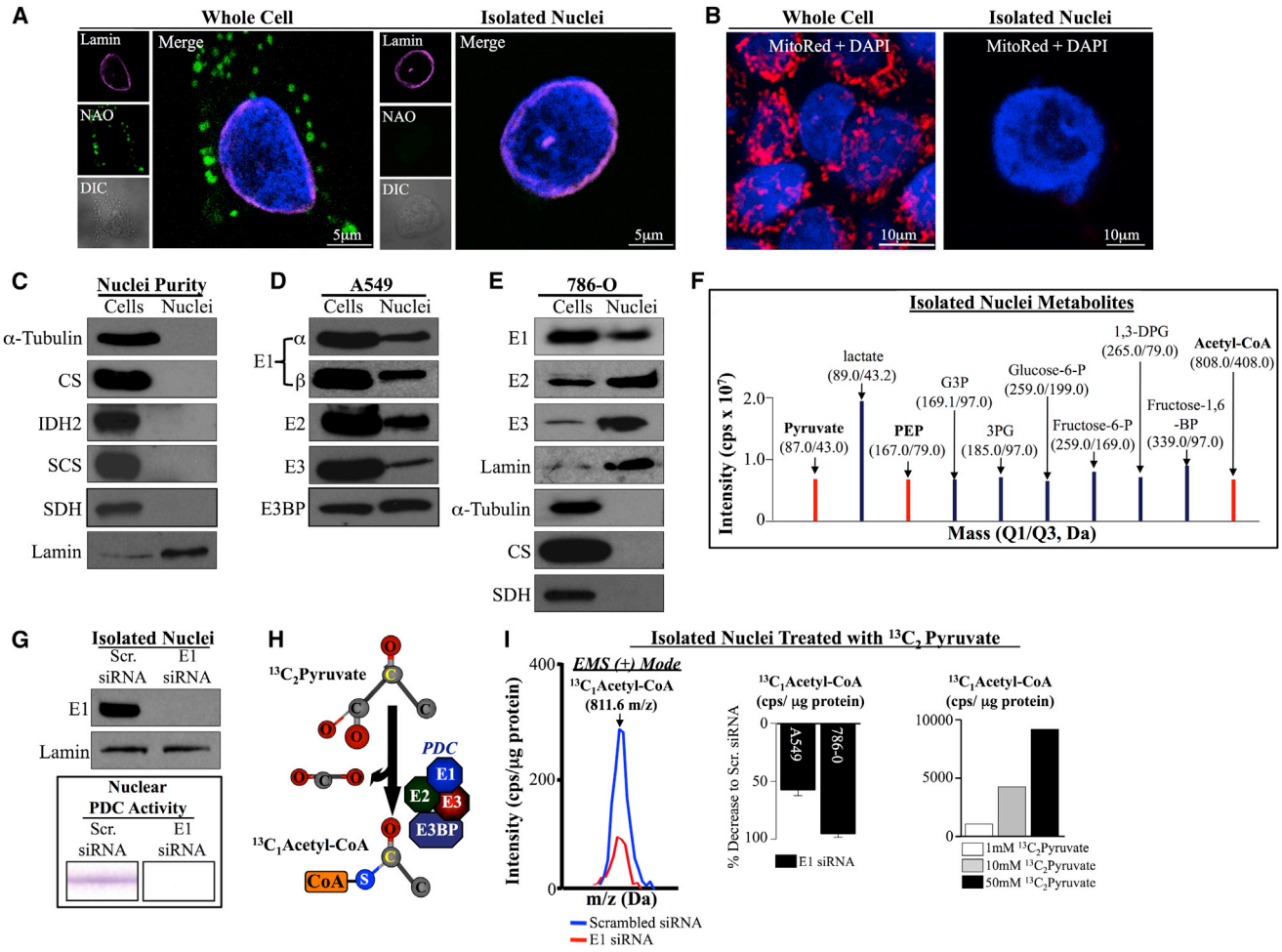

Figure 2. Nuclear PDC Is Functional and Can Synthesize Acetyl-CoA

(A and B) The mitochondrial membrane markers nonyl-acridine orange- (NAO; green; A) and MitoTracker Red- (B) stained whole cells, but signal was not detectable in isolated nuclei preparations. Nuclei were stained with lamin (purple) or DAPI (blue).

(C) Our isolated nuclear preparations had no detectable levels of the cytoplasmic marker α-tubulin and mitochondrial markers citrate synthase (CS), isocitrate dehydrogenase 2 (IDH2), succinyl-CoA synthetase (SCS), and succinate dehydrogenase (SDH) (an example from A549 cells is shown).

(D and E) Immunoblots showing that all subunits of PDC were present in isolated pure nuclei of A549 and 786-O cells.

(F) Many glycolytic intermediates, including phosphoenolpyruvate (PEP), pyruvate, and acetyl-CoA (red), were detected in isolated nuclei from A549 cells, using collision-induced mass spectrometry.

(G) There was no detectable PDC-E1 protein (immunoblot, top) or enzymatic activity measured by a dipstick assay from nuclei isolated from PDC-E1 siRNA-treated cells.

(H) Mechanism for the $^{13}C_2$-pyruvate experiments.

(I) Isolated nuclei from A549 or 786-O cells previously treated with either PDC-E1 or scrambled siRNA were incubated with $^{13}C_2$-pyruvate for 8 hr. The nuclei lacking PDC-E1 had decreased levels of $^{13}C_1$-acetyl-CoA compared to scrambled siRNA controls, measured by mass spectrometry, and normalized to protein concentration. Increasing doses of labeled pyruvate showed a dose-dependent increase in labeled acetyl-CoA.

Error bars represent SEM. See also Figure S2.

preparations reflects the activity of nuclear PDC. We detected a significant decrease in the levels of $^{13}C_1$-labeled acetyl-CoA in nuclei from PDC-E1 siRNA-treated cells compared to those from scrambled siRNA, using two separate mass spectrometry acquisition modes in A549 and 786-O nuclei (Figures 2I and S2C). We also detected increasing levels of labeled acetyl-CoA in response to increasing levels of labeled pyruvate, suggesting the presence of nonlimiting amounts of functional PDC in the isolated nuclei (Figures 2I and S2C).

Nuclear PDC Is Important for Histone Acetylation

We then assessed whether the acetyl-CoA generated from nuclear PDC is important for histone acetylation. Because histone acetylation depends on glucose and not free fatty acid metabolism (Wellen et al., 2009), we first deprived the A549 cells of glucose for 24 hr in order to synchronize acetylation, in the presence of scrambled or PDC-E1 siRNA. Next, we isolated functional nuclei from scrambled and PDC-E1 siRNA-treated cells, exposed them to pyruvate (10 mM) for 8 hr, and measured

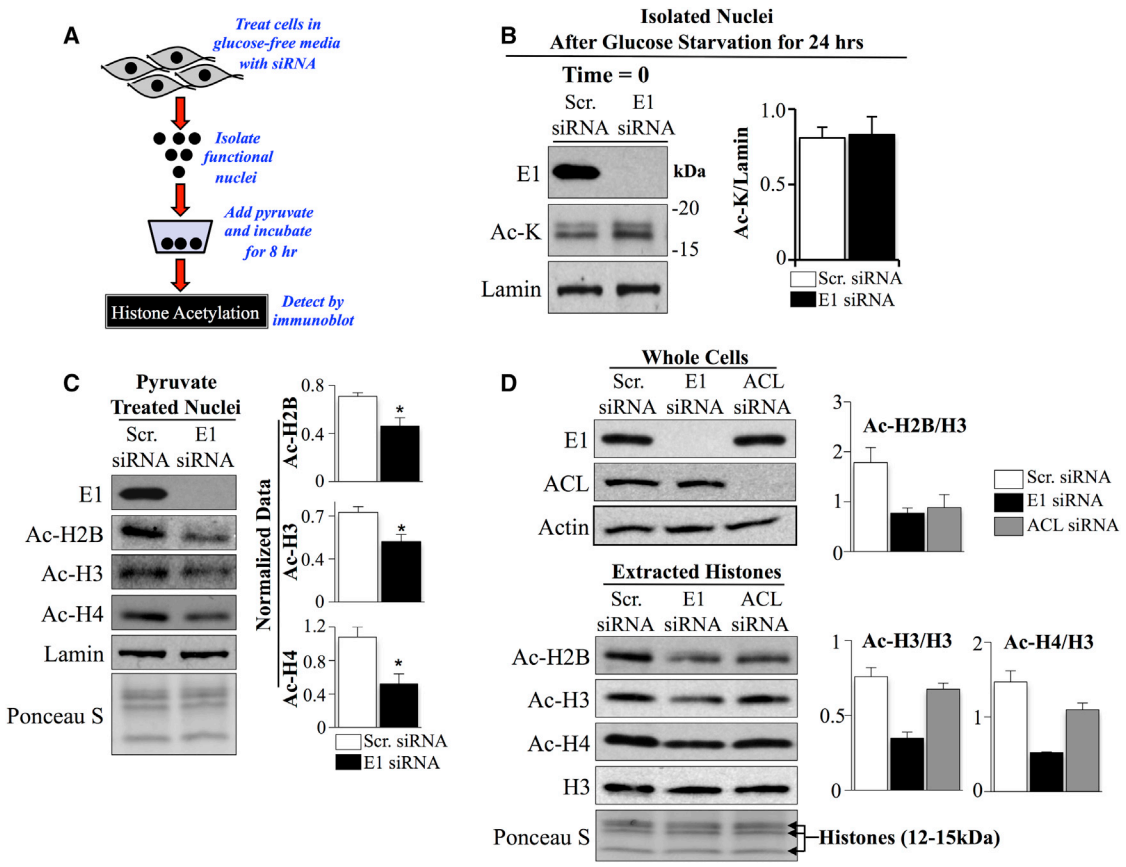

Figure 3. PDC Is Important for Histone Acetylation

(A) Experimental design for acetylation experiments in isolated nuclei.

(B) In the absence of pyruvate at time = 0, there were no differences in acetyl-lysine of proteins within the molecular weight of acetylated histones (n = 3 experiments) between nuclei isolated from PDC-E1 siRNA or scramble-treated cells.

(C) Nuclei lacking PDC-E1 exposed to 10 mM pyruvate for 8 hr had decreased levels of acetylated H2B, H3, and H4, compared to control. Lamin and Ponceau S were loading controls. Representative immunoblots are shown to the left, and quantified mean data normalized to lamin are shown to the right (n = 3 experiments; *$p < 0.05$).

(D) PDC-E1 and ACL siRNA-treated A549 cells had almost complete knockdown of PDC-E1 and ACL, respectively, compared to scrambled siRNA-treated cells (top). Extracted histones from PDC-E1 and ACL siRNA-treated A549 cells exposed to 10 mM glucose had decreased levels of acetylated H2B, H3, and H4 compared to scrambled siRNA control (bottom). Quantified mean data (to total H3) are shown on the right (n = 3 experiments).

Error bars represent SEM. See also Figure S3.

histone acetylation (Figure 3A). Prior to the addition of pyruvate to our isolated nuclei (time = 0), no significant differences were apparent in acetylated lysine levels at the molecular weight of histones between scrambled and PDC-E1 siRNA groups (Figure 3B), confirming the synchronization of acetylation. After exposure to pyruvate, nuclei from PDC-E1 siRNA-treated cells had decreased levels of all three acetylated (Ac) core histones H2B, H3, and H4, compared to nuclei from scrambled siRNA-treated cells (Figure 3C).

On the other hand, inhibition of nuclear PDC did not appear to change the acetylation of p53 and FOXO1 in these cancer cells, suggesting that the acetylation of targets in the nucleus is regulated, perhaps by the availability or proximity of acetyl-transferases or deacetylases with acetyl-CoA-generating enzymes, like PDC (Figure S3). Alternatively, a rapid turnover of acetyl groups in histones, compared to those of other proteins, may also explain why the inhibition of nuclear PDC preferentially showed a decrease in histone acetylation.

Because the role of ACL on nuclear acetylation has not been studied in A549 cells, we used ACL or PDC-E1 siRNA in order to study the relative importance of these two enzymes in nuclear acetylation. Extracted histones from either PDC-E1 or ACL siRNA-treated cells had decreased histone acetylation compared to scrambled siRNA-treated cells (Figure 3D). Nevertheless, in these cells, the impact of PDC-E1 silencing on histone acetylation appears to be larger than that of ACL silencing. This may be explained by the fact that PDC is also involved in the ACL-mediated production of nuclear acetyl-CoA, as mitochondrial PDC is also an important regulator of citrate production (i.e., ACL's substrate) via the Krebs cycle. The effects of ACL and PDC-E1 silencing were not the same on the acetylation of specific histones, suggesting that the

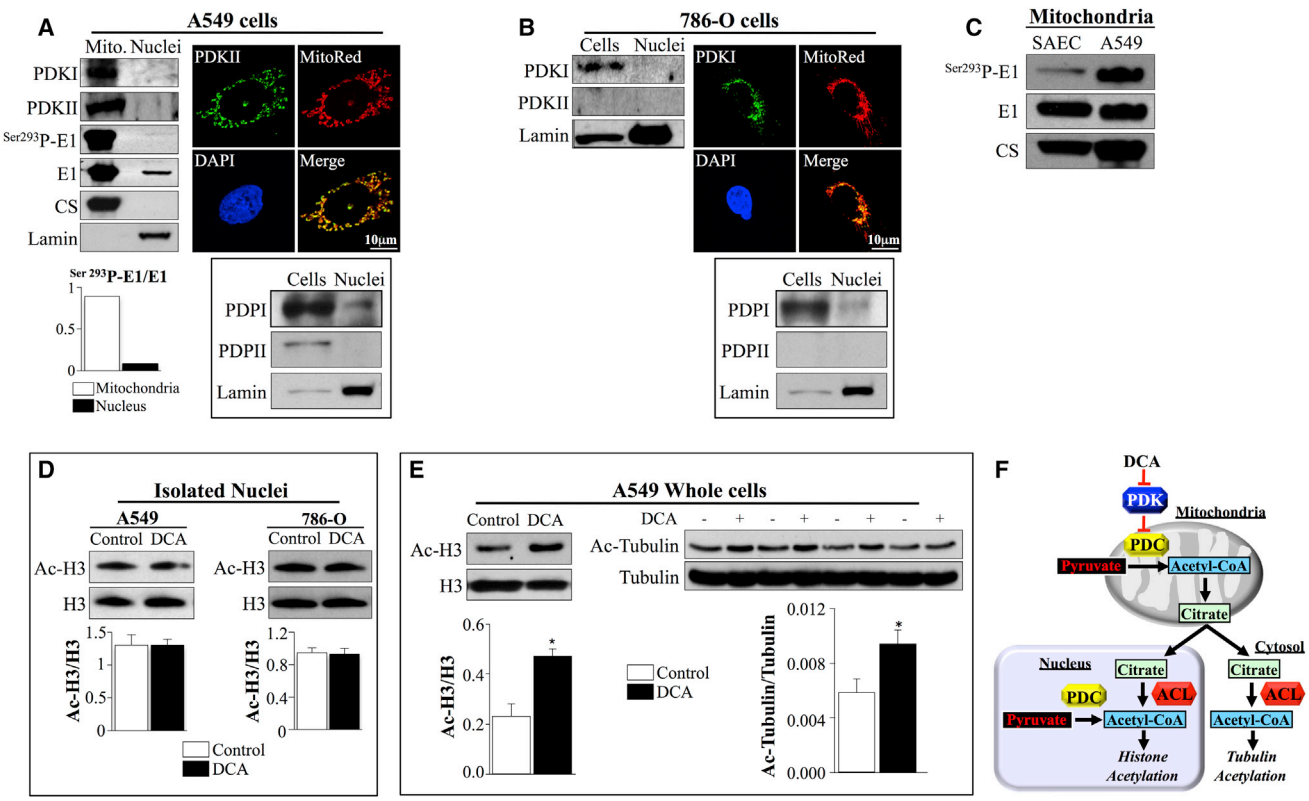

Figure 4. Nuclear PDC Is Regulated Differently Than Mitochondrial PDC

(A) A549 cells have high levels of PDKI and PDKII in isolated mitochondria, but no detectable levels in isolated nuclei. Phosphorylated PDC-E1 serine-293 was present in isolated mitochondria (where PDK is present), but not in isolated nuclei (where PDK is absent), and the ratio of P-E1/E1 is shown below. Confocal microscopy shows the presence of PDKII (green) in the mitochondria as assessed by colocalization (yellow) with MitoTracker Red in the merge panel, but not in the nucleus, stained with DAPI (blue; upper right). Immunoblot showing that PDPI, but not PDPII, is present in isolated nuclei from A549 cells (bottom right).

(B) In 786-O cells, PDKI (but not PDKII) is present in whole cell preparations, but not in isolated nuclei (left). The absence of PDK in the nucleus is confirmed by confocal microscopy (top right). PDPI, but not PDPII, is present in isolated nuclei from 786-O cells (bottom right).

(C) A549 cells had higher levels phosphorylated serine-293 on PDC-E1 compared to isolated mitochondria from normal SAECs.

(D) Extracted histones from isolated A549 (left) and 786-O (right) nuclei exposed to DCA (5 mM) had similar levels of acetylated H3 compared to vehicle-treated control cells.

(E) In contrast, DCA increased the acetylation of H3 (left) and tubulin (right) in whole A549 cells, reflecting the activation of mitochondrial PDC. Representative immunoblots (top) and quantified mean data normalized to total H3 (left) or tubulin (right) are shown (n = 4 experiments; *p < 0.05).

(F) Mechanism for DCA-mediated increase in acetylation (see Results section for discussion).

Error bars represent SEM. See also Figure S4.

source of acetyl-CoA may play a role in which target is acetylated.

Pyruvate Dehydrogenase Kinase Is Not Present in the Nucleus

Mitochondrial PDC-E1 is tonically inhibited by PDKs and activated by PDC phosphatases (PDPs). PDKs phosphorylate serine-293 of the α subunit of PDC-E1, resulting in its inactivation (Behal et al., 1993). Whereas PDK I and II are ubiquitously expressed, PDK III and IV are only expressed in the testis and under starvation conditions in muscle, respectively (Bowker-Kinley et al., 1998). Hypoxia-inducible factor 1α (HIF1α) is activated in many cancers and can suppress mitochondrial PDC by inducing PDK expression (Kim et al., 2006). We detected PDKI and II in mitochondria, but not in isolated nuclei of A549 (which express both isoforms) and 786-O cancer cells (which only express PDKI; Figures 4A and 4B). On the other hand, we detected the presence of PDPI (but not PDPII) in nuclei of A549 and 786-O cells (Figures 4A and 4B). We found higher levels of PDC-E1 serine-293 phosphorylation in A549 mitochondria compared to normal cells (Figure 4C), in keeping with the finding that cancer cells have higher levels of PDK (Michelakis et al., 2010). Furthermore, PDC-E1 phosphorylated serine-293 was present in mitochondria, but not in nuclei (Figure 4A), in keeping with the absence of PDK. This suggested that, in certain conditions (like in cancer or hypoxia, where HIF1α is activated), whereas mitochondrial PDC can be relatively inactive, nuclear PDC could remain constitutively active.

We then treated isolated nuclei from A549 and 786-O cancer cells with the small-molecule PDK inhibitor dichloroacetate

(DCA), which primarily inhibits PDK I and II (Bonnet et al., 2007; Michelakis et al., 2010) and showed no differences in Ac-H3 levels (Figure 4D). However, DCA treatment of whole A549 cells resulted in both increased Ac-H3 (nuclear acetylation) and Ac-tubulin (cytoplasmic acetylation; Figures 4E, S4A, and S4B). The increase in acetylation by DCA in whole cells may be due to acetyl-CoA biosynthesis by cytoplasmic and nuclear ACL, which produces acetyl-CoA using citrate as substrate (Figure 4F). We confirmed the expected DCA-induced increase in citrate, along with another Krebs cycle intermediate (succinate) and the expected decrease in lactate (Figure S4C). Thus, the differential effects of DCA (which has known anticancer properties; Bonnet et al., 2007; Dhar and Lippard, 2009; Michelakis et al., 2010) between mitochondrial and nuclear PDC reflect the differential expression of PDK in the two cellular compartments and suggest that factors that can increase or decrease PDK function (like HIF1α and DCA, respectively) can be used to exploit the functional significance of nuclear PDC, an idea that we explored later on.

PDC Translocates from the Mitochondria to the Nucleus during S Phase

To study whether histone acetylation occurs prior to DNA replication during S phase in our cells, we first synchronized cells to the G1 phase by serum starvation for 24 hr. We then introduced serum and serially measured Ac-H3 and cyclin A. Ac-H3 levels increased first, followed by cyclin A (Figure 5A). By isolating pure nuclei from these cells, we also showed that nuclear PDC-E1 levels followed a similar increase pattern to Ac-H3 and then began to decrease toward baseline, but only after Ac-H3 levels peaked (Figure S5A). Furthermore, using microscopy, we showed that both PDC-E1 and Ac-H3 were higher during late S phase compared to baseline in isolated nuclei (Figure S5B).

We then measured both nuclear and mitochondrial PDC-E1 levels upon serum stimulation after cell cycle synchronization, at the same time points. We found that the increase in nuclear PDC-E1 levels during cell-cycle progression was associated with a parallel decrease in mitochondrial PDC-E1 levels, before both PDC fractions returned toward their baseline levels (Figure 5B). The decrease in mitochondrial PDC was not due to enhanced degradation because PDC levels remained unaltered in whole cells in response to increasing concentrations of serum (Figure S5C), suggesting the decrease in mitochondrial PDC was due to its translocation to the nucleus.

To measure the relative distribution of PDC in the mitochondria and nucleus, we loaded on the same gel the same amount of protein from isolated nuclei and mitochondria at baseline and 3 hr postserum stimulation. Although PDC-E1 levels were clearly higher in mitochondria than the nuclei, the percent ratio of nuclear to mitochondrial PDC-E1 increased from 17% to 30% after 3 hr of serum stimulation (Figure S5D). A similar increase in the percent ratio of nuclear to mitochondrial PDC in response to serum stimulation was also observed with the E2 component using immunofluorescence, where we were able to measure mitochondrial PDC (overlap with MitoRed) and nuclear PDC (overlap with DAPI) within the same cell (Figure 5C).

We then performed a series of experiments to further support the fact that nuclear PDC translocates from the mitochondria. To exclude the possibility that the increase in nuclear PDC in response to serum stimulation is a newly translated product from the endoplasmic reticulum (ER), we inhibited ribosomal translation with cycloheximide (CHX) and measured nuclear PDC levels (see Figure 5D). Serum stimulation increased nuclear PDC (E1 and E2), and this was not altered by CHX, although the translation of c-*myc* (a protein with a short half-life, previously shown to be decreased within 2 hr of CHX treatment; Alarcon-Vargas et al., 2002) was decreased during this timeframe (Figure 5E).

Newly synthesized mitochondrial proteins from the ER contain an N terminus mitochondrial localization sequence (MLS), and upon entry into the matrix, the MLS is cleaved by the mitochondrial-processing peptidase (MPP; see Figure 5D). The cleavage of these (otherwise destabilizing) sequences ($\sim$15–50 amino acids) of mitochondrial proteins is required to prevent degradation and facilitate subsequent assembly of subunits (Chacinska et al., 2009). Only mature (cleaved MLS) PDC proteins are able to refold and form complexes in the mitochondria. Therefore, we hypothesized that, if nuclear PDC is directly translocated to the nucleus after its translation in ribosomes, we should be able to detect the precursor form in the nucleus. Using two separate siRNA transfection approaches for the β-catalytic subunit of MPP, we were able to inhibit the mRNA levels by 65% and 90%, respectively, resulting in the accumulation of increasing levels of the precursor form of PDC-E1 (Figure 5F, see arrowhead) along with the mature form. We then used MPP siRNA-treated whole cells and probed for PDC-E1 on the same membrane with isolated nuclei and mitochondrial protein from untreated cells. Whereas the precursor form was clearly seen in the MPP-silenced whole cells in the same gel, only the mature form of PDC was detected in isolated nuclei and mitochondria (Figure 5G, top). We also isolated nuclei from both scrambled and MPP siRNA-treated cells and could not detect the presence of the precursor; only mature PDC was present in the nucleus (Figure 5G, bottom). As MPP is a mitochondria-specific protease, our data suggest that nuclear PDC is processed in the mitochondria prior to translocation to the nucleus.

All of the subunits of PDC are translated in the ER and are transported separately to the mitochondria, where they are processed prior to complex formation. We hypothesized that, if we inhibit only one of the subunits and thus disturb the stoichiometry balance of the subunits within the complex, we may affect the nuclear levels of the other subunits. Indeed, knockdown of only PDC-E1 by siRNA resulted in decreased levels of all catalytic components of PDC in the nucleus, without changing their overall protein expression in whole cell preparations (Figure S5E). This suggests that PDC is translocated from the mitochondria to the nucleus as a functional complex.

Signals Increasing Nuclear PDC Levels

We then studied signals that may trigger the nuclear translocation of PDC. Epidermal growth factor (EGF) signaling is important for S phase entry and cell-cycle progression (Kato et al., 1998) and has been shown to increase the nuclear translocation

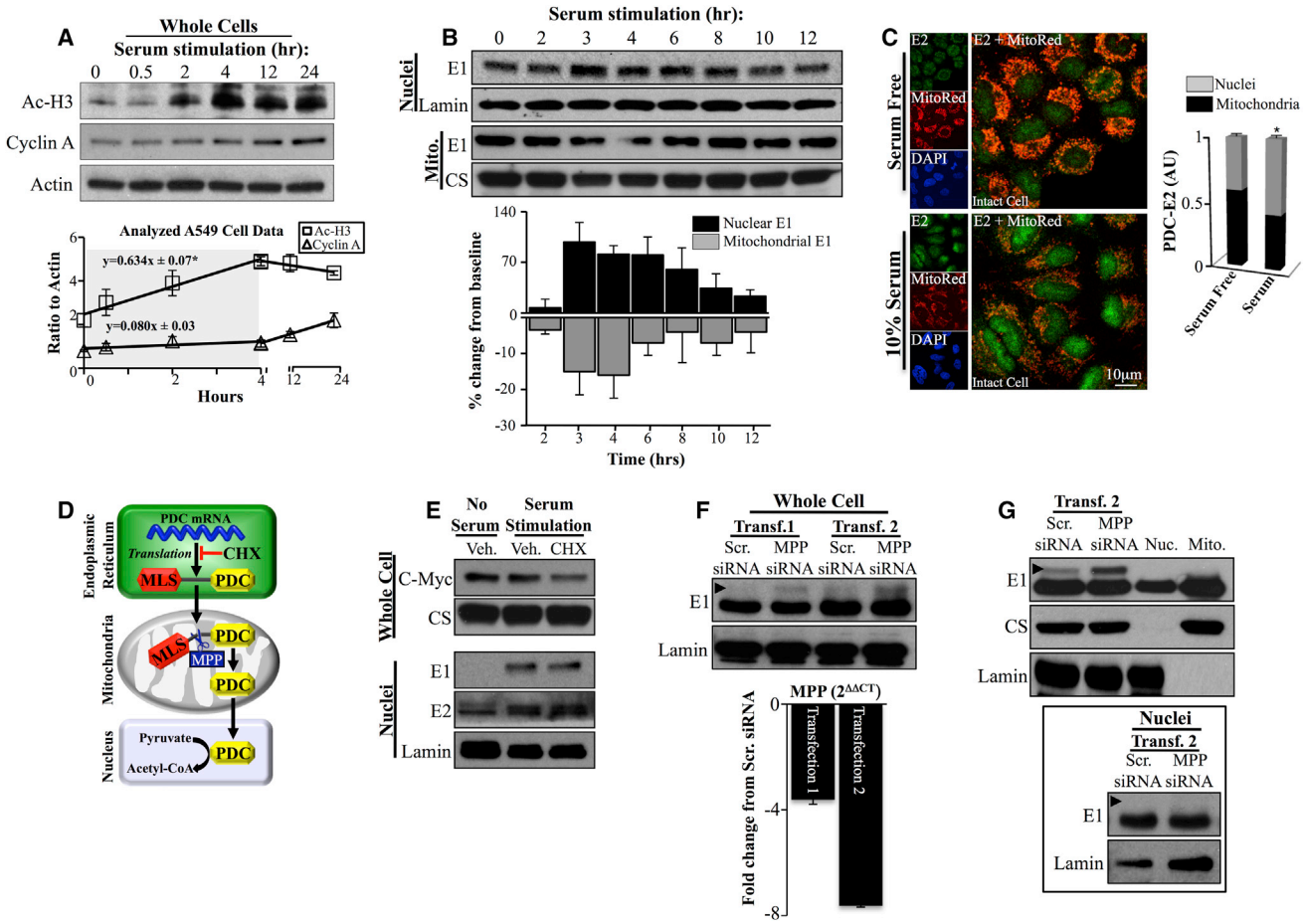

Figure 5. PDC Is Translocated from the Mitochondria to the Nucleus

(A) Serum stimulation time course after cell-cycle synchronization in G1 phase showed an early increase in acetylation of H3, followed by an increase in the S phase marker cyclin A. Representative immunoblots are shown above. The rate of acetylation of H3 is faster than cyclin A expression within the first 4 hr after introduction of serum. Note the brake in the time scale, showing a later relative plateau in H3 acetylation, whereas cyclin A levels continue to increase (n = 3 experiments; *p < 0.001 for Ac-H3 compared to cyclin A slopes).

(B) Serum stimulation time course shows an increase in nuclear levels of PDC-E1 peaking at 3 or 4 hr, associated with a parallel decrease in mitochondrial PDC-E1. This was followed by a return toward baseline levels of both the mitochondrial and nuclear PDC levels. Representative immunoblots are shown above, and quantified data normalized to either lamin (nuclei) or CS (mitochondria) are shown below (n = 4 experiments).

(C) A549 cells were costained with PDC-E2 (green), MitoTracker Red (red), and DAPI (blue). The mitochondrial E2 signal was quantified by signal overlap with MitoTracker Red, whereas nuclear signal was quantified by signal overlap with DAPI in the same cell, and the ratio of the two for each cell was calculated. Serum stimulation increased the nuclear to mitochondrial ratio, suggesting nuclear translocation from mitochondria (n = 25 cells; *p < 0.05).

(D) Experimental design for the study of nuclear PDC translocation using cycloheximide (CHX) and gene silencing of MPP.

(E) In response to serum stimulation (4 hr), nuclear PDC-E1 and PDC-E2 increased, and this was not altered by CHX, which decreased the levels of c-*myc*.

(F) Using two siRNA transfection approaches to silence MPP, we found a clear signal of the unprocessed (precursor) form of PDC-E1 (arrowhead). Lamin was used as a loading control. Quantitative RT-PCR (qRT-PCR) shows the relative fold change for both MPP siRNA transfection approaches. Note that more-effective silencing (transfection 2) resulted in higher levels of the PDC-E1 precursor.

(G) The PDC-E1 precursor was not detected in protein from isolated nuclei or mitochondria loaded in the same gel with whole cell protein from MPP siRNA-treated cells, which clearly showed the presence of the precursor (top; arrowhead shows precursor form). The precursor PDC-E1 was not detectable in nuclei isolated from the MPP siRNA-treated cells (arrowhead represents where the precursor band would have been detected).

Error bars represent SEM. See also Figure S5.

of PKM2 in cancer (Yang et al., 2012). We found that recombinant human EGF (rhEGF) increased the nuclear levels of PDC components, along with PKM2, in A549 cells (Figures 6A and S6A). The increase in nuclear levels was through translocation because rhEGF did not change the total cellular expression of PDC subunits, whereas it predictably increased tyrosine-204 phosphorylation of mitogen-activated protein kinase (MAPK) (Figure 6B). Similarly, gefitinib, an EGF receptor inhibitor, decreased nuclear (Figure 6C), but not whole cell PDC levels (Figure 6D). We then used confocal imaging and studied the relative distribution of PDC subunits within the same cell, in 786-O cells. Similar to A549 cells, rhEGF increased the relative

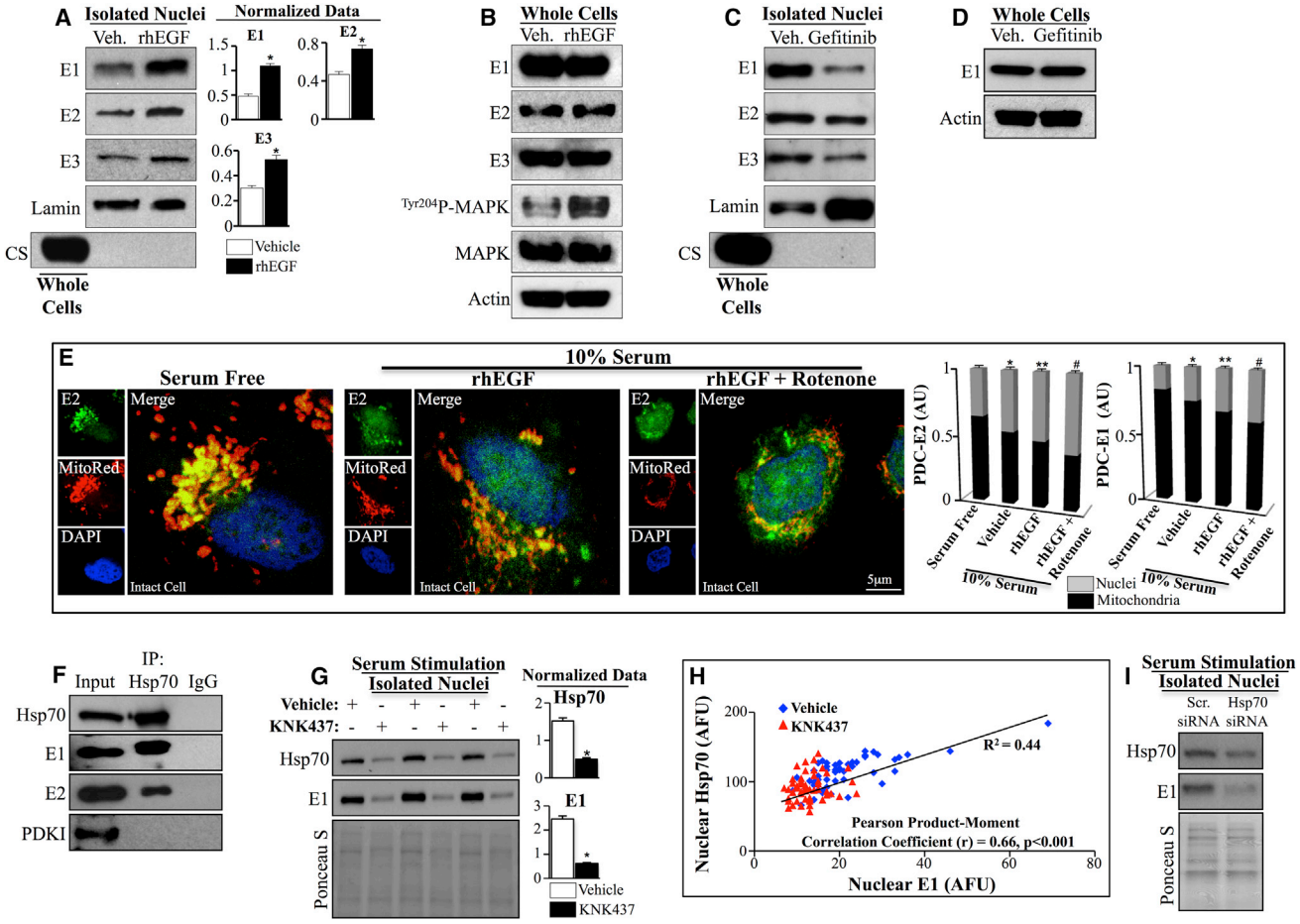

Figure 6. Signals Increasing the Nuclear Translocation of PDC

(A and B) Isolated nuclei from rhEGF-treated A549 cells have increased levels of PDC-E1, E2, and E3 compared to the vehicle-treated cells (n = 3 experiments; *$p < 0.05$; A), without changing total cellular levels, whereas rhEGF treatment increased tyrosine-204 phosphorylation of MAPK (B). Lamin and actin were used as loading controls.

(C and D) Gefitinib decreased nuclear levels of all three PDC subunits, as shown by immunoblots, without changing the total cellular expression.

(E) 786-O cells were costained with PDC-E2 (green), MitoTracker Red (red), and DAPI (blue). Serum stimulation increased the nuclear to mitochondrial ratio, compared to serum-free treated cells; this was enhanced by rhEGF and further enhanced by the addition of rotenone (5 μM; n = 25 cells; *$p < 0.05$ compared to serum free; **$p < 0.05$ compared to vehicle; #$p < 0.05$ compared to rhEGF). A similar pattern was seen in PDC-E1translocation (representative images shown in Figure S6B).

(F) Hsp70 coimmunoprecipitates with PDC-E1 and PDC-E2, but not with PDKI, in A549 cells. Input represents 2.5 μg of whole cell lysate. IP, immunoprecipitation.

(G) Serum-stimulated (4 hr) A549 cells pretreated with KNK437 (100 μM) show decreased nuclear levels of both Hsp70 and PDC-E1 compared to vehicle (DMSO)-treated cells. Mean data are normalized to Ponceau S (n = 3 experiments; *$p > 0.05$).

(H) The same cells as in (G) were costained with Hsp70 and PDC-E1, imaged with confocal microscopy, and the nuclear fluorescence intensity was measured. A Pearson product-moment correlation plot showed that nuclear levels of Hsp70 and PDC-E1 correlate positively ($r = 0.66$; $p < 0.001$; n = 50 cells/group). Representative images are shown in Figure S6H. AFU, arbitrary fluorescence units.

(I) Serum-stimulated (4 hr) A549 cells transfected with Hsp70 siRNA show decreased nuclear levels of both Hsp70 and PDC-E1, compared to scrambled-transfected cells.

Error bars represent SEM.

distribution of PDC-E1 and PDC-E2 from the mitochondria to the nucleus (Figure 6E).

We speculated that a mitochondrial stressor might trigger translocation of PDC from the mitochondria to the nucleus. We studied the electron transport chain (ETC) complex I inhibitor rotenone, because inhibition of ETC complexes is a well-known cause of mitochondrial stress (Durieux et al., 2011). We found that rotenone caused a significant translocation of PDC into the nucleus over and above serum and rhEGF (Figures 6E and S6B). Mitochondria adapt to stress by initiating the mitochondria unfolded protein response, which results in increased expression of mitochondrial import proteins, folding chaperones and heat shock proteins, amplifying the communication with the nucleus (Zhao et al., 2002). We speculated that a heat shock chaperone may be involved in the nuclear translocation of PDC.

We studied heat shock protein 70 (Hsp70) based on evidence that (1) induction of Hsp70 is cell cycle dependent, with its highest expression and nuclear localization observed during S phase (Milarski and Morimoto, 1986), (2) Hsp70 is involved in the nuclear translocation of several proteins (Shi and Thomas, 1992), and (3) Hsp70 binds to and activates mitochondrial PDC (Kiang et al., 2006). We confirmed that nuclear levels of Hsp70 increase in a cell-cycle-dependent manner, similarly to the increase in nuclear PDC-E1 following serum stimulation (Figure S6C). We performed immunoprecipitation studies on A549 cells and MRC-9 cells (fibroblasts) with Hsp70 and detected the presence of PDC-E1 and PDC-E2 (Figures 6F and S6D), suggesting that Hsp70 may bind to these components of the complex. Sequence and structural analysis of potential binding motifs for Hsp70 within the PDC complex showed a putative Hsp70-binding motif (i.e., hydrophobic peptide regions; Mayer and Bukau, 2005) within the PDK-binding site on PDC (Figure S6E). PDK did not coimmunoprecipitate with Hsp70 (Figures 6F and S6D), suggesting that Hsp70 and PDK may compete for similar binding domains within PDC.

We pretreated serum-starved A549 and 786-O cells with either vehicle (DMSO) or KNK437, an inhibitor of heat shock factor 1, which results in decreased expression of inducible Hsp70 (Koishi et al., 2001), prior to serum stimulation for 4 hr. KNK437 decreased mRNA expression (Figure S6F) and nuclear levels of both Hsp70 and PDC-E1, compared to vehicle (Figures 6G and S6G). Nuclear Hsp70 levels correlated positively with nuclear PDC-E1 levels in both vehicle and KNK437-treated A549 cells (Figures 6H and S6H). Similar to KNK437, a specific siRNA against Hsp70 also decreased nuclear levels of both Hsp70 and PDC-E1 in response to serum stimulation (Figure 6I).

Nuclear PDC Is Important for S Phase Entry and Cell-Cycle Progression

Our data on the dynamic translocation of PDC from the mitochondria to the nucleus suggest that it is the same enzymatic complex that is present in both compartments, rather than perhaps a different variant. This makes the study of the relative biological role of PDC on histone acetylation and cell-cycle progression in the two cellular compartments challenging, particularly in the intact cell setting. We took advantage of PDK's localization in mitochondria, but not the nucleus, and designed experiments in an intact cell setting, in which by subtracting the effects of selective mitochondrial PDC inhibition (by the induction of PDK) from the effects of total cellular PDC inhibition (by PDC-E1 siRNA), we could expose the role of nuclear PDC.

Whereas PDK is already induced in cancer cells, we aimed to maximally inhibit mitochondrial PDC by two methods: first, inducing endogenous PDK by activation of HIF1α and, second, increasing exogenous PDKI via transfection with a PDKI plasmid (see Figure 7A). With either method, mitochondrial PDC should be maximally inhibited (condition 1). Then, by inhibiting total cellular PDC by siRNA gene silencing (condition 2), we could expose the effects of nuclear PDC on histone acetylation and cell-cycle progression by subtracting condition 1 from condition 2 (Figure 7A).

For the first experiment, we infected A549 cells with an adenovirus encoding for CA5 (AdCA5), a constitutively active mutant form of HIF1α (mHIF1α) (Manalo et al., 2005), avoiding the confounding effects of hypoxia. Compared to an adenovirus encoding for LacZ (AdLacZ), increased expression of mHIF1α by AdCA5 (Figures S7A and S7B) resulted in a significant increase in the expression of PDKI (Figure 7B) and phosphorylation of serine-293 on mitochondrial, but not nuclear, PDC-E1 (Figure 7C). Mutant HIF1α increased mitochondrial membrane potential (Figure S7C), further supporting the mitochondrial PDC suppression and its impact on mitochondrial function in our model, as we have previously described (Bonnet et al., 2007). We then treated AdCA5-infected cells with scrambled (condition 1) versus PDC-E1 siRNA (condition 2). We also gave scrambled siRNA to AdLacZ-infected cells (control). We synchronized all the groups to the G1 phase by serum starvation for 24 hr, followed by reintroduction of serum, and 24 hr later, we measured S phase markers and specific histone-3 acetylation sites that are involved in cell-cycle progression. AdCA5-infected cells treated with scrambled siRNA had increased acetylation of H3K9 and H3K18, both important for S phase progression (Cai et al., 2011); increased G1-S phase progression shown by increased levels of phosphorylated retinoblastoma (P-Rb); as well as elongation-2 factor (E2F), cyclin A, and cyclin-dependent kinase 2 (Cdk2), markers for S phase entry, compared to AdLacZ-infected cells treated with scrambled siRNA (Figure 7D). These effects (condition 1) are in agreement with the described effects of HIF1α on proliferation (Semenza, 2010) and the recruitment of histone acetyl transferases (Luo et al., 2011). In contrast, AdCA5-infected cells treated with PDC-E1 siRNA (condition 2) had significantly decreased acetylation of H3K9 and H3K18 and decreased levels of P-Rb, E2F, cyclin A, and Cdk2 compared to AdCA5-infected cells treated with scrambled siRNA (condition 1; Figure 7D). Because both conditions had activated HIF1α and inhibited mitochondrial PDC, subtraction of condition 2 (gray bars) from condition 1 (black bars) in Figure 7D shows that nuclear PDC inhibition decreases Ac-H3K9 and Ac-H3K18 (whereas total H3 levels remain relatively stable) as well as P-Rb and S phase regulators (E2F, cyclin A, and Cdk2).

For the second experiment, transfection with a PDKI plasmid increased the expression of PDKI (Figure S7D) and phosphorylation of PDC-E1 serine-293 (Figure 7E), compared to the empty vector control. PDKI overexpression did not change histone acetylation or cell-cycle progression (Figure 7E; compare white bars [control] to black bars [condition 1]), compatible with the fact that mitochondrial PDC is significantly inhibited in these cancer cells at baseline and further inhibition may not elicit any measurable effects. However, similar to the first experiment, PDC siRNA (condition 2), decreased H3K9 and H3K18 acetylation and decreased P-Rb, E2F, cyclin A, and Cdk2, compared to scrambled siRNA controls (condition 1; Figure 7E). Thus, two different approaches of inhibiting nuclear PDC support its role in S phase progression.

DISCUSSION

Here, we show that PDC is present and functional in the nucleus. Nuclear PDC can generate acetyl-CoA utilized for histone acetylation and S phase entry, providing a link between metabolism and epigenetic or cell-cycle regulation. This source of nuclear

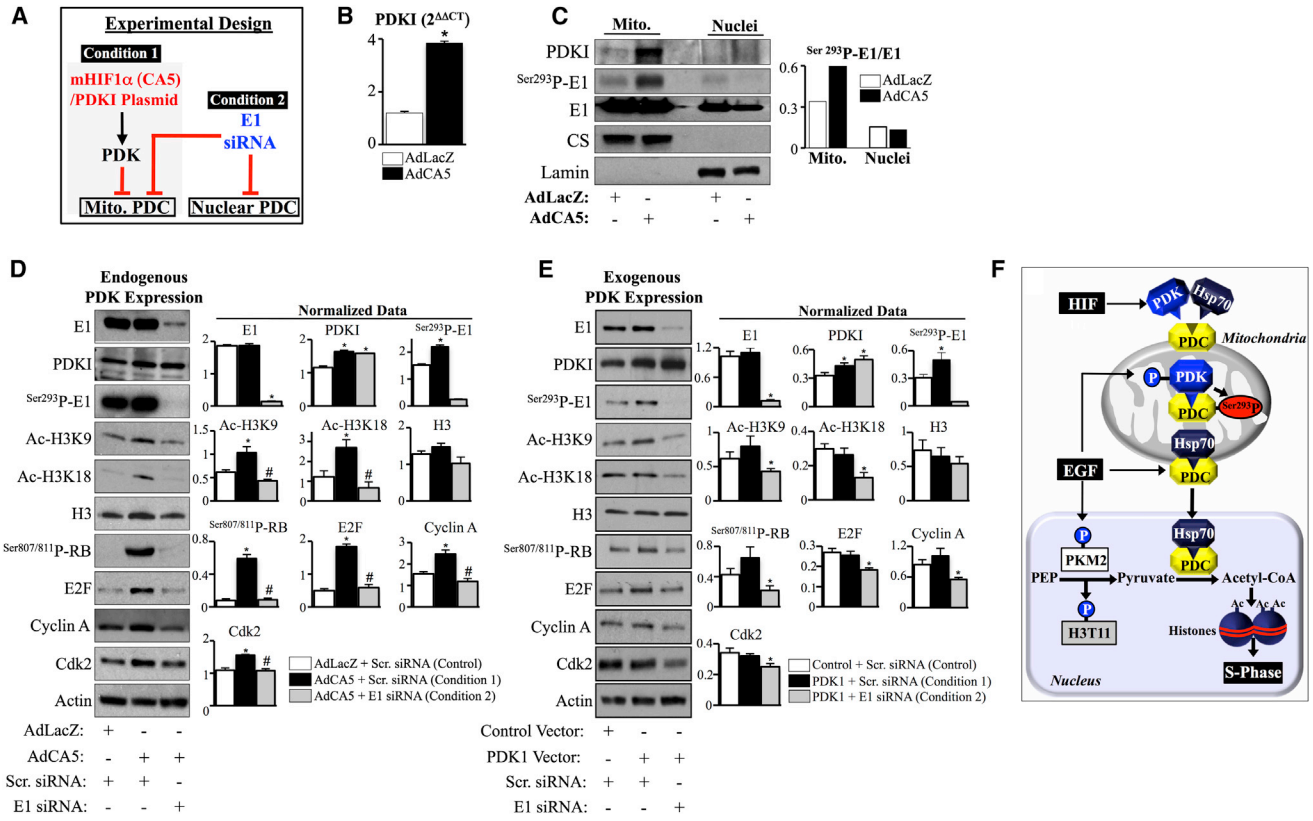

Figure 7. Nuclear PDC Is Important for S Phase Entry

(A) Experimental design for the study of nuclear PDC on S phase entry in whole cells (see Results section).

(B and C) AdCA5-treated cells had higher PDKI mRNA levels (n = 3 experiments; *p < 0.01) and higher PDKI protein levels and phosphorylated PDC-E1 serine-293 compared to AdLacZ-treated cells in isolated mitochondria, but no detectable levels of PDKI were seen in isolated nuclei from both groups compared to AdLacZ-treated cells (quantification of the immunoblots is shown to the right).

(D) A549 cells treated with AdCA5 (condition 1) followed by scrambled siRNA had increased levels of PDKI; phosphorylated PDC-E1; Ac-H3K9; Ac-H3K18; the G1-S phase progression marker P-Rb; and the S phase markers elongation-2 factor (E2F), cyclin A, and cyclin-dependent kinase 2 (Cdk2) compared to AdLacZ-treated scrambled siRNA cells. In contrast, A549 cells treated with AdCA5 followed by PDC-E1 siRNA (condition 2) had decreased levels of both PDC-E1 and phosphorylated PDC-E1; similar levels of PDK; and decreased levels of Ac-H3K9, Ac-H3K18, P-Rb, E2F, cyclin A, and Cdk2 compared to AdCA5-treated scrambled siRNA cells (n = 3 experiments; *p < 0.05 versus AdLacZ scr. siRNA; #p < 0.05 versus AdCA5 scr. siRNA).

(E) Transfection with PDKI plasmid followed by PDC-E1 siRNA (condition 2) decreased the levels of PDC-E1, phosphorylated PDC-E1, Ac-H3K9, Ac-H3K18, P-Rb, E2F, cyclin A, and Cdk2 compared to transfection with PDKI plasmid but treated with scrambled siRNA (condition 1; n = 3 experiments; *p < 0.05 versus scr. siRNA).

(F) Proposed model for the translocation of PDC from mitochondria to the nucleus and its functional role (see Discussion).

Error bars represent SEM. See also Figure S7.

acetyl-CoA may also be important in conditions where the availability of cytoplasmic citrate (which can cross the nuclear membrane and produce acetyl-CoA through ACL) is decreased due to suppressed production or shift toward lipid synthesis. Our work suggests that nuclear PDC has a mitochondrial origin because it lacks the MLS (which can only be cleaved in the mitochondria), and its nuclear increase in response to serum is not affected by inhibition of ribosomal translation. In addition to serum, nuclear PDC translocation increases under growth factors (EGF) or mitochondrial inhibitors (rotenone), suggesting a potential role in disease states with proliferative signals or mitochondrial dysfunction, like cancer.

It is intriguing that our data suggest translocation of PDC in the nucleus, given the large size of this enzymatic complex. High-resolution electron microscopy and structural analysis have recorded its size and diameter within the range of 8–10 MDa and 25–45 nm, respectively (Sumegi et al., 1987; Zhou et al., 2001a). However, there is evidence for size and conformational variability of PDC with identification of complexes as small as 1 MDa (Sumegi et al., 1987; Zhou et al., 2001b). Although the stoichiometry of the individual components in the complex (i.e., the relative amount of E1, E2, and E3 subunits) varies, in keeping with the reported variability in its size among tissues, only the interplay of all subunits within a functional complex can produce acetyl-CoA. The fact that we find de novo production of acetyl-CoA in isolated nuclei in response to pyruvate suggests that a functional complex is present. The fact that we can decrease the nuclear levels of all subunits by only silencing the gene for one subunit suggests that the complex travels as a whole from the mitochondria into the nucleus. PDC was recently identified

as an intact functional complex on the outer mitochondrial membrane (Hitosugi et al., 2011), suggesting that it can translocate across mitochondrial membranes, a more complex process than translocation across the nuclear membrane. Because the nuclear pore complex can accommodate the entry of large complexes of similar diameter to PDC, like ribonucleoprotein complexes (Lodish et al., 2000) or intact nucleocapsids of viruses (Panté and Kann, 2002), it is possible that an intact PDC complex could translocate to the nucleus.

We provide evidence that Hsp70 may promote the nuclear translocation of a constitutively active form of PDC. By competing with PDK for binding to PDC, Hsp70 may allow PDC to remain active when translocated to the nucleus (Figure 7F). Kiang et al. (2006) showed that Hsp70 binds to and activates mitochondrial PDC, but did not show the mechanism of this activation. It may be that, by competing with PDK, Hsp70 inhibits the binding of this inhibitory kinase and thus activates PDC. It is possible that EGF can promote nuclear acetylation by a coordinated translocation of PKM2 and PDC, potentially by increasing Hsp70 levels (Milarski and Morimoto, 1986; Figure 7F). This model may contribute to the recently described effects of nuclear PKM2 on tumor growth via histone acetylation, offering a source and mechanism for the nuclear acetyl-CoA generation used for the acetylation of H3K9 (Yang et al., 2012). It is appealing to consider that there is a mechanism by which several factors required for the nuclear response to proliferative stimuli (for example PKM2 and PDC) can be transferred simultaneously, increasing efficiency. Although our collective data support the existence of the translocation model shown in Figure 7F, we cannot rule out the possibility that individual subunits may be transported independently in the nucleus, where they could potentially be assembled in an intact complex with the help of a chaperone, like Hsp70.

Tyrosine phosphorylation by growth factor signaling, including EGFR, activates PDKI, providing a mechanism for suppression of mitochondrial PDC in cancer (Hitosugi et al., 2011), in addition to the induction of PDK expression by HIF1α (Kim et al., 2006). Therefore, in a ''double hit'' manner, EGF stimulation can activate PDK, suppressing mitochondrial PDC (which has been shown to inhibit mitochondria-dependent apoptosis in cancer; Bonnet et al., 2007) in tandem with Hsp70-mediated nuclear translocation of PDC, promoting histone acetylation and cell-cycle progression (Figure 7F). The inhibition of PDK by siRNA, DCA, or hybrid drugs (like mitoplatin, a drug that structurally combines cisplatin with DCA molecules; Dhar and Lippard, 2009) decreases cancer growth in animal models (Bonnet et al., 2007) and a small human trial (Michelakis et al., 2010) by activating glucose oxidation, reversing the Warburg effect and the resistance to apoptosis in cancer cells. Our work now suggests that the nuclear pool of PDC is ''immune'' to this strategy. It raises the possibility that, in response to these interventions, cancer cells may ''escape'' by promoting a transfer of PDC in the nucleus, where PDC may promote proliferation. It also suggests that anticancer strategies, in which PDK inhibition is used, may perhaps be strengthened by simultaneous inhibition of EGFR signaling or Hsp70 function. As PDC plays a prominent role in many metabolic disorders, it will be important for scientists to be aware that their efforts to target PDC may have direct and previously unrecognized effects on nuclear biology.

Our work suggests an alternative pathway to ACL for the nucleus to generate acetyl-CoA for histone acetylation. It is possible that, in specific tissues or disease states, the relative importance of ACL or nuclear PDC may be different. ACL has been shown to be important for histone acetylation during differentiation (Wellen et al., 2009), whereas our work suggests that histone acetylation by nuclear PDC may be important for cell-cycle progression. ACL and PDC should be studied together when assessing histone acetylation and epigenetic regulation in conditions in which both differentiation and proliferation are taking place, including development, cancer, and other proliferative conditions or stem cell biology.

EXPERIMENTAL PROCEDURES

For additional details, see Extended Experimental Procedures.

Cell Culture

Human A549 non-small-cell lung cancer cells, 786-O renal cell carcinoma, and MRC-9 fibroblasts were purchased from ATCC. A549 cells were maintained on F12K medium, whereas 786-O cells in RPMI-1640 media and MRC-9 cells in Eagle's minimal essential medium (EMEM). Primary human fibroblasts were isolated from the lung of a transplant patient in accordance with the Human Ethics Committee at the University of Alberta and maintained in Dulbecco's modified Eagle's medium (DMEM). Human SAECs were purchased from ScienCell and maintained in SAEpiCM, provided by the company. Media for all cell lines were supplemented with 10% fetal bovine serum (FBS) (unless stated otherwise) and 5% antibiotic and antimycotic (Invitrogen-Gibco Canada).

Confocal Microscopy

Confocal microscopy was performed using a two-photon Zeiss LSM 510 NLO model (Carl Zeiss). All images were scanned in midplane of the cell in the z axis as shown in Figure 1D, using a 100× numerical aperture (NA) 1.3 oil objective lens at 2× zoom, allowing for a pixel size of 0.04 × 0.04 × 0.2 μm. Fluorophore-conjugated secondary antibodies (Dako, Invitrogen, and Molecular Probes) and the nuclear stain DAPI (Molecular Probes) were used for immunofluorescence imaging with specific excitations of 488 nm (Fitc), 543 (Tritc), 633 (Far Red), and 750 nm; two photon (DAPI) and the corresponding emissions were detected with the following filter sets. Fitc: band pass (BP) 505–535; Tritc: BP 565–615; Far red: high pass (LP) 650; and DAPI: BP 390–465. Overlap was eliminated between the emissions of any secondary antibodies, mitochondrial-specific dyes, EGFP, and nuclear stains by imaging each channel independently and sequentially with only one excitation wavelength active during each scan.

Mass Spectrometry for $^{13}C_1$-acetyl-CoA

Isolated nuclei from scrambled and PDC-E1 siRNA-treated cells were exposed to $^{13}C_2$-pyruvate (Cambridge Isotope Laboratories) for 8 hr, before the experiment was terminated with the addition of ice-cold storage buffer. Metabolites were extracted and 30 μl of samples was diluted to 120 μl with methanol and flow injected to the mass spectrometry (MS) using 4000 QTRAP mass spectrometer (AB Sciex) with either enhanced product ion (EPI; IonSpray voltage of −4,500 V) or enhanced MS (EMS; IonSpray voltage of 5,500 V).

Immunoblotting

Immunoblotting with standard SDS-PAGE was performed as previously described (Bonnet et al., 2007). Where required, SDS-PAGE of purified histones as well as nuclear, mitochondrial, and cellular protein was performed on 16.5% Tricine gels (Bio-Rad) followed by immunoblotting to low-pore-size (0.2 μm) nitrocellulose (Bio-Rad).

Statistical Analysis

Unpaired Student's t test was used for statistical calculations when comparing the effects of treatment between two sample groups. Error bars indicate SEM.

SUPPLEMENTAL INFORMATION

Supplemental Information includes Extended Experimental Procedures, seven figures, and two movies and can be found with this article online at http://dx.doi.org/10.1016/j.cell.2014.04.046.

ACKNOWLEDGMENTS

We would like to thank Dr. Ryan McKay of the Canadian National High Field NMR Centre (NANUC) and Chenomx for the NMR acquisition and data analysis, Dr. Nasser Tahbaz (University of Alberta) for the immunogold labeling and electron microscopy, and Dr. Gregg Semenza (Johns Hopkins University) for the adenoviruses encoding LacZ and CA5. This study was funded by the Canadian Institutes for Health Research, the Alberta Innovation for Health Solutions, and the Hecht Foundation (Vancouver, Canada) to E.D.M.

Received: December 1, 2013
Revised: March 19, 2014
Accepted: April 18, 2014
Published: July 3, 2014

REFERENCES

Alarcon-Vargas, D., Tansey, W.P., and Ronai, Z. (2002). Regulation of c-myc stability by selective stress conditions and by MEKK1 requires aa 127-189 of c-myc. Oncogene *21*, 4384–4391.

Behal, R.H., Buxton, D.B., Robertson, J.G., and Olson, M.S. (1993). Regulation of the pyruvate dehydrogenase multienzyme complex. Annu. Rev. Nutr. *13*, 497–520.

Bonnet, S., Archer, S.L., Allalunis-Turner, J., Haromy, A., Beaulieu, C., Thompson, R., Lee, C.T., Lopaschuk, G.D., Puttagunta, L., Bonnet, S., et al. (2007). A mitochondria-K+ channel axis is suppressed in cancer and its normalization promotes apoptosis and inhibits cancer growth. Cancer Cell *11*, 37–51.

Bowker-Kinley, M.M., Davis, W.I., Wu, P., Harris, R.A., and Popov, K.M. (1998). Evidence for existence of tissue-specific regulation of the mammalian pyruvate dehydrogenase complex. Biochem. J. *329*, 191–196.

Cai, L., Sutter, B.M., Li, B., and Tu, B.P. (2011). Acetyl-CoA induces cell growth and proliferation by promoting the acetylation of histones at growth genes. Mol. Cell *42*, 426–437.

Chacinska, A., Koehler, C.M., Milenkovic, D., Lithgow, T., and Pfanner, N. (2009). Importing mitochondrial proteins: machineries and mechanisms. Cell *138*, 628–644.

Choudhary, C., Kumar, C., Gnad, F., Nielsen, M.L., Rehman, M., Walther, T.C., Olsen, J.V., and Mann, M. (2009). Lysine acetylation targets protein complexes and co-regulates major cellular functions. Science *325*, 834–840.

Dhar, S., and Lippard, S.J. (2009). Mitaplatin, a potent fusion of cisplatin and the orphan drug dichloroacetate. Proc. Natl. Acad. Sci. USA *106*, 22199–22204.

Durieux, J., Wolff, S., and Dillin, A. (2011). The cell-non-autonomous nature of electron transport chain-mediated longevity. Cell *144*, 79–91.

Gao, X., Wang, H., Yang, J.J., Liu, X., and Liu, Z.R. (2012). Pyruvate kinase M2 regulates gene transcription by acting as a protein kinase. Mol. Cell *45*, 598–609.

Hitosugi, T., Fan, J., Chung, T.W., Lythgoe, K., Wang, X., Xie, J., Ge, Q., Gu, T.L., Polakiewicz, R.D., Roesel, J.L., et al. (2011). Tyrosine phosphorylation of mitochondrial pyruvate dehydrogenase kinase 1 is important for cancer metabolism. Mol. Cell *44*, 864–877.

Horner, D.S., Hirt, R.P., and Embley, T.M. (1999). A single eubacterial origin of eukaryotic pyruvate: ferredoxin oxidoreductase genes: implications for the evolution of anaerobic eukaryotes. Mol. Biol. Evol. *16*, 1280–1291.

Jaenisch, R., and Bird, A. (2003). Epigenetic regulation of gene expression: how the genome integrates intrinsic and environmental signals. Nat. Genet. Suppl. *33*, 245–254.

Kato, Y., Tapping, R.I., Huang, S., Watson, M.H., Ulevitch, R.J., and Lee, J.D. (1998). Bmk1/Erk5 is required for cell proliferation induced by epidermal growth factor. Nature *395*, 713–716.

Kiang, J.G., Bowman, P.D., Lu, X., Li, Y., Ding, X.Z., Zhao, B., Juang, Y.T., Atkins, J.L., and Tsokos, G.C. (2006). Geldanamycin prevents hemorrhage-induced ATP loss by overexpressing inducible HSP70 and activating pyruvate dehydrogenase. Am. J. Physiol. Gastrointest. Liver Physiol. *291*, G117–G127.

Kim, J.W., and Dang, C.V. (2005). Multifaceted roles of glycolytic enzymes. Trends Biochem. Sci. *30*, 142–150.

Kim, J.W., Tchernyshyov, I., Semenza, G.L., and Dang, C.V. (2006). HIF-1-mediated expression of pyruvate dehydrogenase kinase: a metabolic switch required for cellular adaptation to hypoxia. Cell Metab. *3*, 177–185.

Koishi, M., Yokota, S., Mae, T., Nishimura, Y., Kanamori, S., Horii, N., Shibuya, K., Sasai, K., and Hiraoka, M. (2001). The effects of KNK437, a novel inhibitor of heat shock protein synthesis, on the acquisition of thermotolerance in a murine transplantable tumor in vivo. Clin. Cancer Res. *7*, 215–219.

Lodish, H., Berk, A., Zipursky, S.L., Matsudaira, P., Baltimore, D., and Darnell, J. (2000). 4, Signal-Mediated Transport through Nuclear Pore Complexes. In Molecular Cell Biology, Fourth Edition, W.H. Freeman, ed. (New York: W.H. Freemand and Company).

Luo, W., Hu, H., Chang, R., Zhong, J., Knabel, M., O'Meally, R., Cole, R.N., Pandey, A., and Semenza, G.L. (2011). Pyruvate kinase M2 is a PHD3-stimulated coactivator for hypoxia-inducible factor 1. Cell *145*, 732–744.

Manalo, D.J., Rowan, A., Lavoie, T., Natarajan, L., Kelly, B.D., Ye, S.Q., Garcia, J.G., and Semenza, G.L. (2005). Transcriptional regulation of vascular endothelial cell responses to hypoxia by HIF-1. Blood *105*, 659–669.

Mayer, M.P., and Bukau, B. (2005). Hsp70 chaperones: cellular functions and molecular mechanism. Cell. Mol. Life Sci. *62*, 670–684.

Michelakis, E.D., Sutendra, G., Dromparis, P., Webster, L., Haromy, A., Niven, E., Maguire, C., Gammer, T.L., Mackey, J.R., Fulton, D., et al. (2010). Metabolic modulation of glioblastoma with dichloroacetate. Sci. Transl. Med. *2*, 31ra34.

Milarski, K.L., and Morimoto, R.I. (1986). Expression of human HSP70 during the synthetic phase of the cell cycle. Proc. Natl. Acad. Sci. USA *83*, 9517–9521.

Panté, N., and Kann, M. (2002). Nuclear pore complex is able to transport macromolecules with diameters of about 39 nm. Mol. Biol. Cell *13*, 425–434.

Rodríguez, M.A., García-Pérez, R.M., Mendoza, L., Sánchez, T., Guillen, N., and Orozco, E. (1998). The pyruvate:ferredoxin oxidoreductase enzyme is located in the plasma membrane and in a cytoplasmic structure in Entamoeba. Microb. Pathog. *25*, 1–10.

Semenza, G.L. (2010). Defining the role of hypoxia-inducible factor 1 in cancer biology and therapeutics. Oncogene *29*, 625–634.

Shi, Y., and Thomas, J.O. (1992). The transport of proteins into the nucleus requires the 70-kilodalton heat shock protein or its cytosolic cognate. Mol. Cell. Biol. *12*, 2186–2192.

Siebert, G., and Humphrey, G.B. (1965). Enzymology of the nucleus. Adv. Enzymol. Relat. Areas Mol. Biol. *27*, 239–288.

Sumegi, B., Liposits, Z., Inman, L., Paull, W.K., and Srere, P.A. (1987). Electron microscopic study on the size of pyruvate dehydrogenase complex in situ. Eur. J. Biochem. *169*, 223–230.

Vander Heiden, M.G., Locasale, J.W., Swanson, K.D., Sharfi, H., Heffron, G.J., Amador-Noguez, D., Christofk, H.R., Wagner, G., Rabinowitz, J.D., Asara, J.M., and Cantley, L.C. (2010). Evidence for an alternative glycolytic pathway in rapidly proliferating cells. Science *329*, 1492–1499.

Vogelauer, M., Rubbi, L., Lucas, I., Brewer, B.J., and Grunstein, M. (2002). Histone acetylation regulates the time of replication origin firing. Mol. Cell *10*, 1223–1233.

Wellen, K.E., Hatzivassiliou, G., Sachdeva, U.M., Bui, T.V., Cross, J.R., and Thompson, C.B. (2009). ATP-citrate lyase links cellular metabolism to histone acetylation. Science *324*, 1076–1080.

Yang, W., Xia, Y., Hawke, D., Li, X., Liang, J., Xing, D., Aldape, K., Hunter, T., Alfred Yung, W.K., and Lu, Z. (2012). PKM2 phosphorylates histone H3 and promotes gene transcription and tumorigenesis. Cell *150*, 685–696.

Yi, C.H., Pan, H., Seebacher, J., Jang, I.H., Hyberts, S.G., Heffron, G.J., Vander Heiden, M.G., Yang, R., Li, F., Locasale, J.W., et al. (2011). Metabolic regulation of protein N-alpha-acetylation by Bcl-xL promotes cell survival. Cell *146*, 607–620.

Yogev, O., Yogev, O., Singer, E., Shaulian, E., Goldberg, M., Fox, T.D., and Pines, O. (2010). Fumarase: a mitochondrial metabolic enzyme and a cytosolic/nuclear component of the DNA damage response. PLoS Biol. *8*, e1000328.

Zhao, Q., Wang, J., Levichkin, I.V., Stasinopoulos, S., Ryan, M.T., and Hoogenraad, N.J. (2002). A mitochondrial specific stress response in mammalian cells. EMBO J. *21*, 4411–4419.

Zhou, Z.H., McCarthy, D.B., O'Connor, C.M., Reed, L.J., and Stoops, J.K. (2001a). The remarkable structural and functional organization of the eukaryotic pyruvate dehydrogenase complexes. Proc. Natl. Acad. Sci. USA *98*, 14802–14807.

Zhou, Z.H., Liao, W., Cheng, R.H., Lawson, J.E., McCarthy, D.B., Reed, L.J., and Stoops, J.K. (2001b). Direct evidence for the size and conformational variability of the pyruvate dehydrogenase complex revealed by three-dimensional electron microscopy. The "breathing" core and its functional relationship to protein dynamics. J. Biol. Chem. *276*, 21704–21713.